Directional emission of single photons from small atomic samples

Yevhen Miroshnychenko,[1] Uffe V. Poulsen,[2] and Klaus Mølmer[1]
[1]*Lundbeck Foundation Theoretical Center for Quantum System Research, Department of Physics and Astronomy, University of Aarhus, DK-8000 Aarhus C, Denmark*
[2]*Department of Engineering, University of Aarhus, DK-8200 Aarhus N, Denmark*
(Received 28 August 2012; published 19 February 2013)

We provide a formalism to describe deterministic emission of single photons with tailored spatial and temporal profiles from a regular array of multilevel atoms. We assume that a single collective excitation is initially shared by all the atoms in a metastable atomic state and that this state is coupled by a classical laser field to an optically excited state which rapidly decays to the ground atomic state. Our model accounts for the different field polarization components via reabsorption and emission of light by the Zeeman manifold of optically excited states.

DOI: 10.1103/PhysRevA.87.023821 PACS number(s): 42.50.Nn, 42.50.Ct, 42.50.Ex, 03.67.Hk

I. INTRODUCTION

Single photons may serve as flying qubits to communicate between registers of stationary, material qubits in quantum computing architectures [1], and they may be applied in protocols for quantum cryptography. In these protocols transmission losses over long distances can be counteracted by the transfer of the light-state qubits to quantum repeaters for purification and entanglement distillation [2]. Candidates for stationary qubits that can effectively interact with single photons are optically thick ensembles of atoms [3–8], rare-earth ions in crystals [9–12], vibrational excitations in diamond crystals [13], and systems with fewer particles using optical cavities to increase the interaction with the photon field [14–18]. The systems mentioned can provide a deterministic coupling of the material system to a suitably tailored spatial and temporal photon wave packet. There are also a number of probabilistic protocols, where measurement processes herald the successful generation of nonclassical excitations of either the photon field or the medium [19–21]. In this article we utilize the fact that an ensemble of just a few hundred atoms may interact strongly with a single mode of light with a specifically chosen mode function. We identify this mode function by calculating the emitted field from the atomic ensemble, prepared in a collectively excited state. By a time-reversal argument, the complex conjugate of this emitted field may be injected on a ground-state atomic ensemble and will then be fully absorbed at a definite instant of time [22,23]. We discuss the possibility of shaping the temporal profile of the emitted photon and, in particular, the creation of time-symmetric photon wave packets, as such packets can then be emitted by one ensemble and absorbed by another one in a fully deterministic manner. We focus on samples of a few hundred atoms, distributed over a few-micrometer spatial extent. In such ensembles, the Rydberg blockade interaction may be used to establish singly excited states and, subsequently, single-photon states [8,24–29], while photonic qubits, collectively absorbed by the atoms, may be manipulated by Rydberg state mediated quantum gate operations [22,30,31].

The collective interaction of light with ensembles of absorbers and scatterers has been an active field of study since the early days of electromagnetism, while collective phenomena in spontaneous emission received wide attention with the pioneering work on Dicke superradiance from population inverted samples [32]. Early studies of collective emission from ensembles with few excitations [33–37] (see also Ref. [38], and references therein) have been followed by a recent flourishing of analyses [22,39–46], which apply a Born-Markov approximation and eliminate the field degrees of freedom to obtain coupled equations for the atomic excited-state amplitudes. Approximate solutions to these equations may be derived, e.g., with the assumption of a scalar description of the field; for only a few hundred atoms, they may also be solved directly on a computer.

In this article we generalize the previous analyses to account for the full vector character of the quantized radiation field. We establish coupled equations for excited-state amplitudes on a suitable set of atomic Zeeman sublevels, emitting and reabsorbing the different polarization components of the field, and we solve the equations numerically to identify the full temporal, spatial, and polarization contents of the emitted light.

In Sec. II we derive the coupled atomic equations under the Born-Markov approximation. In Sec. III, we present numerical results for the photon modes emitted by samples of atoms with different spatial geometries. In Sec. IV, we describe the use of a coupling laser field to control the temporal shape of the emitted photon wave packet, and in Sec. V, we present a brief conclusion and outlook of the work.

II. DIPOLE-DIPOLE INTERACTION

We want to describe the experimental situation where a collection of N atoms can be prepared in a single ground state g and where a suitable, symmetric excitation mechanism allows the preparation of a state

$$|\psi\rangle = \sum_{j=1}^{N} a_j |g_1 g_2 \ldots, f_j, \ldots g_N\rangle \tag{1}$$

with a single atom transferred to the metastable state f; see Fig. 1. The Rydberg blockade mechanism may restrict the system to a single excitation [27–29], but in the present article we shall assume the state in Eq. (1) as the starting point for our analysis and pay no further attention to its exact preparation mechanism. We assume that N atoms are located at the positions $\vec{r}_j$ ($j = 1, \ldots, N$), and with plane-wave

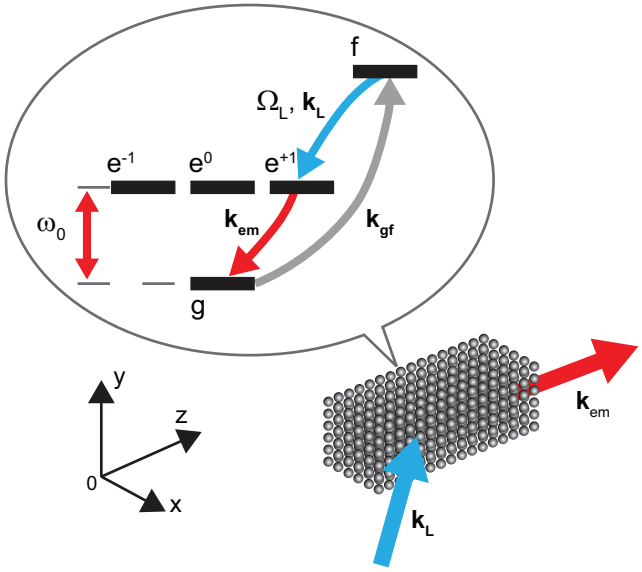

FIG. 1. (Color online) Atoms with three excited substates, e^{-1}, e^0, and e^{+1}, a ground state g, and a long-lived state f are arranged in a regular lattice. State f is coupled to state e^{+1} by a classical laser field. The excited states decay to the ground state, emitting a photon with σ^-, π, and σ^+ polarized photons, respectively. The direction of the emission is determined by the wave number of the atomic g-f coherence and the wave number of the out-coupling field, $\vec{k}_{em} = -\vec{k}_{gf} - \vec{k}_L$.

excitation laser fields, the amplitudes have equal magnitude and phases, $\exp(i\vec{k}_{gf}\cdot\vec{r}_j)$, given by the phase of the fields at the atomic locations. For convenience we will incorporate the phase of the out-coupling field with wave number $\vec{k}_L$ in the definition of the atomic excited-state amplitudes, $a_j = \frac{1}{\sqrt{N}}\exp[i(\vec{k}_{gf}+\vec{k}_L)\cdot\vec{r}_j]$. This allows us to describe the interaction between the atoms and the outcoupling laser with a real Rabi frequency Ω_L. State f, sketched in Fig. 1, may indeed represent a long-lived Rydberg state or a long-lived low-lying atomic state reached by a Raman process via a Rydberg state.

To release a photon from the system, we use a classical laser field with the Rabi frequency Ω_L to drive the atomic f-state amplitude into an optically excited state e, with a strong dipole coupling to the ground state g. The system now acts as an antenna array for dipole radiation on the e-g transition, and this is the cause of the desired directionality of the emitted light. As indicated in Fig. 1, the initially populated states may be extremal Zeeman sublevels with well-defined polarization selection rules, and the photon emitted on the e-g transition may be σ^+ polarized with respect to the atomic quantization axis. This field, however, may be reabsorbed by another atom located in an arbitrary direction from the emitter, and here, the expansion of the field on polarization components permits excitation with selection rules $\Delta m = 0,\pm1$. To describe the many-atom emission, we thus have to consider other ground and excited Zeeman sublevels than the ones initially populated.

A closed transition in an alkali-metal atom, such as the $5^2S_{1/2}\ |F=2,m_F=+2\rangle$ transition to $5^2P_{3/2}\ |F=3,m_F=+3\rangle$ in ^{87}Rb, is a suitable candidate for the $|g\rangle$ to $|e^{+1}\rangle$ transition depicted in Fig. 1. The collective enhancement of decay towards state $|g\rangle$ initially populated by all but one of the atoms and the initial feeding of the extremal Zeeman level limit the amount of the population transferred to other ground states and motivate the restriction of our model to a single ground state g, the metastable state f, and three excited states, e^0, $e^{\pm1}$, depicted with the thick solid lines in Fig. 1. The dipole coupling strength between g and the three excited states depend on the specific hyperfine states of the different alkali atoms, and for simplicity, we assume identical couplings, which corresponds to the case of a $J=0-J=1$ optical transition. Alternatively, one could use a closed transition $^1S_0$ to $^1P_1$ in bosonic isotopes of alkaline-earth-metal (e.g., Sr) or rare-earth (e.g., Yb) atoms. This level configuration is the simplest realistic model that allows us to take the polarization of the emitted and reabsorbed light as well as the resulting dipole-dipole interactions between the atoms into account. In the following we will use the shorthand notation $|f_j\rangle \equiv |g_1 g_2\cdots f_j\cdots g_N\rangle$ for singly excited states of the atomic ensemble and similar notation for $|e^\nu\rangle$, with $\nu = 0,\pm1$.

In the dipole approximation the interaction of atoms with photons is described by a Hamiltonian [34]:

$$\hat{H} = \hat{H}_0 + \hat{H}_{\rm int}, \tag{2}$$

where

$$\hat{H}_0 = \sum_{\vec{k}}\sum_{\lambda}\hbar\omega_k a^+_{\vec{k}\lambda}a_{\vec{k}\lambda} + \sum_{j=1}^{N}\sum_{\nu=-1}^{1}\hbar\omega_0|e^\nu_j\rangle\langle e^\nu_j| + \sum_{j=0}^{N}\hbar\omega_{fg}|f_j\rangle\langle f_j| \tag{3}$$

is the atom-field Hamiltonian and the interaction part is

$$\hat{H}_{\rm int} = \hat{H}_L + \hat{H}_V. \tag{4}$$

The semiclassical coupling to the initial long-lived state is

$$\hat{H}_L = \sum_{j=1}^{N}\hbar\frac{\Omega_L}{2}\left[(\vec{\sigma}^j_{fe}\cdot\vec{\epsilon}_L)e^{-i\omega_L t} + (\vec{\sigma}^j_{ef}\cdot\vec{\epsilon}_L)e^{i\omega_L t}\right], \tag{5}$$

where $\vec{\epsilon}_L$ is the polarization direction of the coupling field with the optical frequency ω_L and $\vec{\sigma}^j_{fe} = \hat{d}_{fe}|f_j\rangle\langle e^{+1}_j|$. We further assume the direction of the dipole moment for this transition $\hat{d}_{fe}$ to be parallel to $\vec{\epsilon}_L$, so that the transfer of amplitude happens exclusively to the state $|e^{+1}\rangle$.

The coupling of the atomic dipole between $|g\rangle$ and $|e\rangle$ to the quantized radiation field modes is described by

$$\hat{H}_V = -i\sum_{j=1}^{N}\sum_{\vec{k}}\sum_{\lambda}\hbar g_k\left[(\vec{\sigma}^j_{eg}\cdot\vec{\epsilon}_{\vec{k}\lambda})a_{\vec{k}\lambda}e^{i\vec{k}\cdot\vec{r}_j} - (\vec{\sigma}^j_{ge}\cdot\vec{\epsilon}_{\vec{k}\lambda})a^+_{\vec{k}\lambda}e^{-i\vec{k}\cdot\vec{r}_j}\right]. \tag{6}$$

Here, the atomic dipole operator is defined as $\vec{\sigma}^j_{ge} = \sum_{\nu=-1}^{1}\hat{d}^j_{g\nu}|g\rangle\langle e^\nu_j|$, where $\hat{d}^j_{g\nu}$ is the unit vector in the direction of the corresponding dipole moment for the $|g\rangle$-$|e^\nu\rangle$ transition. $a_{\vec{k}\lambda}$ is the annihilation operator of a vacuum electromagnetic field mode $\vec{k}$ with the polarization λ in the direction $\vec{\epsilon}_{\vec{k}\lambda}$. The atom-field coupling strength is $g_k = d_{eg}(\frac{\omega_k}{2\varepsilon_0\hbar V})^{1/2}$, with dipole moment d_{eg}, quantization volume V, and $\omega_k = ck$.

We henceforth ignore spontaneous emission on the e-f transition. This may, on the one hand, be chosen as a transition

with a weaker dipole moment, and on the other hand, it does not experience the collective enhancement that we shall observe on the e-g transition.

We expand the time-dependent solution of the Schrödinger equation for N atoms and the field as a superposition of Fock states with a single atomic or photonic excitation:

$$|\psi(t)\rangle = \sum_{j=1}^{N} a_j(t) e^{-i\omega_{fg}t} |f_j\rangle|0\rangle + \sum_{j=1}^{N}\sum_{\nu=-1}^{+1} \beta_j^{\nu}(t) e^{-i\omega_0 t} |e_j^{\nu}\rangle|0\rangle + \sum_{\vec{k}}\sum_{\lambda} e_{\vec{k}\lambda}(t) e^{-i\omega_k t} |g\rangle|1_{\vec{k},\lambda}\rangle, \tag{7}$$

where $|g\rangle$ represents the state with all atoms in the ground state.

Note that we use the rotating-wave approximation (RWA) in Eq. (5) because we treat this transition semiclassically. In the quantized atom-light interaction described by Eq. (6), the direct application of RWA considerably simplifies the equations, but as it neglects virtual photon contributions, it leads to a wrong dipole-dipole interaction term in the final equation. For the case of two-level atoms, however, it was observed [29,36] that the virtual photon contribution to the atom-atom interaction terms can be correctly recovered by handling the sum over wave-number field modes in Eq. (7) in spherical coordinates and by extending the radial integral over modes artificially to include negative photon frequencies $\omega = ck < 0$. A generalization of this analysis to the case of multilevel atoms interacting with a quantized vector field, which will be presented elsewhere [47], allows us to apply the same procedure in our treatment of the quantized atom-light interaction in Eq. (6).

Substitution of Eq. (7) with the initial condition $e_{\vec{k}\lambda}(0) = 0$ into the Schrödinger equation with the Hamiltonian from Eq. (2) yields the formal solution

$$e_{\vec{q}\sigma}(t) = \sum_{j=1}^{N}\sum_{\nu=-1}^{+1} g_q e^{-i\vec{q}\cdot\vec{r}_j} \left(\hat{d}_{g\nu}^{j} \cdot \vec{\epsilon}_{\vec{q}\sigma}\right) \int_0^t d\tau \beta_j^{\nu}(\tau) e^{-i(\omega_0-\omega_q)\tau}. \tag{8}$$

Using the Markovian approximation [33] the atomic coefficient $\beta_j^{\nu}(\tau)$ can be approximated by $\beta_j^{\nu}(t)$ in Eq. (8) and taken outside the integral. This allows us to substitute the photon amplitudes by expressions involving only atomic state amplitudes, which thus obey a closed set of equations:

$$\dot{a}_l = \frac{\Omega_L}{2i} e^{i(\omega_{fe}-\omega_L)t} \beta_l^{+1}, \tag{9}$$

$$\dot{\beta}_l^{\eta} = \frac{\Omega_L}{2i} e^{-i(\omega_{fe}-\omega_L)t} \delta_{\eta,1} a_l - \left(\frac{\Gamma}{2} - i\Delta_{\mathrm{Lamb}}\right)\beta_l^{\eta} - \frac{\Gamma}{2}\sum_{j=1}^{N}\sum_{\nu=-1}^{1}(1-\delta_{l,j})\left(\hat{d}_{\eta g}^{l} \cdot \overleftrightarrow{F}_{l,j} \cdot \hat{d}_{g\nu}^{j}\right)\beta_j^{\nu}. \tag{10}$$

Here Γ is the single-atom decay rate from $|e\rangle$ to $|g\rangle$, and Δ_{Lamb} is the single-atom Lamb shift. This term contains an infinite integral, where a suitable cutoff should be applied to yield a finite physical value [48]. After this procedure, this shift is absorbed into the definition (the measured value) of the energy of the atomic state $|e\rangle$ in Eq. (7). The second-rank tensor $\overleftrightarrow{F}_{l,j} = \overleftrightarrow{f}(k_0 R_{l,j}) - i\overleftrightarrow{g}(k_0 R_{l,j})$ with

$$\overleftrightarrow{f}(kR) = \frac{3}{2}\left(\overleftrightarrow{I} - \hat{R}\hat{R}\right)\frac{\sin(kR)}{kR} + \frac{3}{2}\left(\overleftrightarrow{I} - 3\hat{R}\hat{R}\right)\left(\frac{\cos(kR)}{(kR)^2} - \frac{\sin(kR)}{(kR)^3}\right), \tag{11}$$

$$\overleftrightarrow{g}(kR) = \frac{3}{2}\left(\overleftrightarrow{I} - \hat{R}\hat{R}\right)\frac{\cos(kR)}{kR} - \frac{3}{2}\left(\overleftrightarrow{I} - 3\hat{R}\hat{R}\right)\left(\frac{\sin(kR)}{(kR)^2} + \frac{\cos(kR)}{(kR)^3}\right), \tag{12}$$

$k_0 = \omega_0/c$. and $\vec{R}_{l,j} = \vec{r}_l - \vec{r}_j$ accounts for the field-mediated interaction between atoms l and j. Here, $\overleftrightarrow{I}$ is the unity tensor, and $\hat{R}\hat{R}$ is the projection onto the direction given by $\vec{R}$ [33].

Equations (9) and (10) account for the zero-photon subspace component of the total wave function of the atoms and the quantized field,

$$|\Psi_0(t)\rangle = \sum_{j=1}^{N} a_j(t)|f_j\rangle + \sum_{j=1}^{N}\sum_{\nu=-1}^{+1}\beta_j^{\nu}(t)|e_j^{\nu}\rangle, \tag{13}$$

and this state component is described by an effective non-Hermitian Hamiltonian

$$\hat{H}^{\mathrm{eff}} = \hat{H}_0^{\mathrm{eff}} + \hat{H}_L^{\mathrm{eff}} + \hat{H}_{dd}^{\mathrm{eff}}, \tag{14}$$

with

$$\hat{H}_0^{\mathrm{eff}} = -i\hbar\left(\frac{\Gamma}{2} - i\Delta_{\mathrm{Lamb}}\right)\sum_{l=1}^{N}\sum_{\eta=-1}^{+1}|e_l^{\eta}\rangle\langle e_l^{\eta}| \tag{15}$$

describing individual single-atom effects,

$$\hat{H}_L^{\mathrm{eff}} = -\frac{\hbar\Omega_L}{2}\sum_{l=1}^{N} e^{i(\omega_{fe}-\omega_L)t}|f_l\rangle\langle e_l^{+1}| + \mathrm{H.c.} \tag{16}$$

giving the coupling from the long-lived state f, and

$$\hat{H}_{dd}^{\mathrm{eff}} = i\hbar\frac{\Gamma}{2}\sum_{j,l=1}^{N}\sum_{\nu,\eta=-1}^{+1}(1-\delta_{l,j}) \times\left(\hat{d}_{\eta g}^{l} \cdot \overleftrightarrow{F}_{l,j} \cdot \hat{d}_{g\nu}^{j}\right)|e_j^{\eta}\rangle\langle e_j^{\nu}| \tag{17}$$

expressing collective dispersive and dissipative effects between the atoms in the ensemble.

In the rest of this paper we are interested in the spatial and temporal emission profiles. The $\overleftrightarrow{g}$ part of $\overleftrightarrow{F}$ defines the Hermitian part of $\hat{H}_{dd}^{\mathrm{eff}}$, i.e., the coherent exchange of excitation between the atoms. The $\overleftrightarrow{f}$ part conversely defines the anti-Hermitian part corresponding to the decay by the emission of light and thus the population of the one-photon quantum-state component. If the Hermitian part is diagonalized, delocalized orthogonal eigenmodes with collectively "Lamb-shifted" energies are obtained. If the anti-Hermitian part is diagonalized, delocalized orthogonal independently decaying modes are obtained. Some of these modes have a decay time longer than Γ (i.e., they are Dicke subradiant modes [32]), and some decay faster than Γ (i.e., they are Dicke superradiant modes; see Refs. [22,39], and references therein). The Hermitian and the anti-Hermitian parts do not commute, and hence the eigenmodes of the full Hamiltonian $\hat{H}^{\mathrm{eff}}$, which

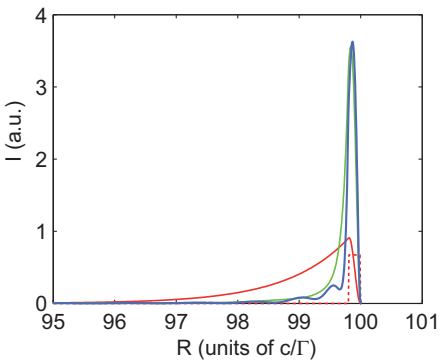

FIG. 2. (Color online) A snapshot of the total intensity emitted by a cloud of $14 \times 14 \times 10$ (blue) and $3 \times 3 \times 10$ (green) atoms with the lattice spacing $d = 0.25\lambda_0$ and a single atom (red) using a square out-coupling pulse indicated by the dotted line. The larger atomic ensembles experience the faster decay and the sharpest emission peaks. Parameters used for this simulation are $\Omega_L = 8.2\Gamma$, a vanishing single atom detuning of the the Ω_L light field, and a coupling pulse length $t_w = 0.2\Gamma^{-1}$.

provide the time-dependent atomic state as a single sum of complex exponentially weighted vectors, are *not* orthogonal. This will result in coupling between different decay channels and a quantum beatlike behavior for the decay modes [43]. The blue line in Fig. 2 shows a snapshot of emitted intensity integrated over all directions at different distances from a cloud of $14 \times 14 \times 10$ atoms excited from the levels $|f_j\rangle$ to the levels $|e_j^{+1}\rangle$ by a square Ω_L pulse. The dotted line in Fig. 2 indicates the timing of the out-coupling square pulse. The initial emission rate is faster than the single-atom emission rate Γ presented by the red (medium gray) line. Additionally, we see a modulation of the emitted intensity due to the coupling of the different nonorthogonal decay modes. With the reduction of the cloud size, the coupling between the decay modes becomes weaker, but the superradiance behavior remains pronounced, as shown by the green (light gray) line in Fig. 2 for the array of only $3 \times 3 \times 10$ atoms. For comparison, we show [red (medium gray) curve] also the emission by a single atom.

III. SPATIAL PHOTON MODES

The eigenmode expansion of Eqs. (9) and (10) for the atomic excitation amplitudes formally yields a solution for each individual atomic excited-state amplitude as a sum of exponential functions of time with complex arguments. Once the atomic evolution is determined, the light emission is given by the integrals in Eq. (8). We note that for the relevant time scales, which are longer than the ensemble excited-state lifetime, these integrals involve only decaying exponential functions, and they may, in practice, be extended to infinity. This allows us to determine the (far) field eigenmode expansion coefficients as algebraic expressions involving the mode expansion coefficients divided by the sum of the complex eigenvalues and the frequency difference appearing explicitly in Eq. (8). This means that we can readily determine the field amplitudes on any chosen set of field modes after diagonalization of the atomic problem, at a cost that depends only on the number of atoms, and calculations with even thousands of atoms are realistic.

The probability to detect a photon at a position $\vec{r}$ at time instance t, which is much later than L/c, where L is the linear sample length, is given by [49]

$$I_\epsilon(\vec{r},t) = \langle \psi(t)|E_\epsilon^{(-)}(\vec{r})E_\epsilon^{(+)}(\vec{r})|\psi(t)\rangle. \tag{18}$$

Here ϵ is the handedness of the photon, i.e., its circular polarization along the line connecting the atomic ensemble and the detector at position $\vec{r}$. The positive frequency component of the desired polarization is given by $E_\epsilon^{(+)}(\vec{r}) = [\vec{\epsilon}\cdot\vec{E}^{(+)}(\vec{r})]$, with [34]

$$\vec{E}^{(+)}(\vec{r}) = i\sum_{\vec{q}}\sum_{\sigma}\varepsilon_q \vec{\epsilon}_{\vec{q},\sigma} a_{\vec{q},\sigma} e^{i\vec{q}\cdot\vec{r}} \tag{19}$$

and $\varepsilon_q = (\frac{\hbar\omega_q}{2\varepsilon_0 V})^{1/2}$. See Appendix A for the full derivation of I_ϵ.

In this section we assume that the atomic system is initially prepared in a so-called timed Dicke state,

$$a_j(0) = \frac{1}{\sqrt{N}} e^{-i\vec{r}_j\cdot\vec{k}_{gf}}, \quad \beta_j^\nu(0) = 0. \tag{20}$$

This state is coupled to $|e^{+1}\rangle$ by switching on the laser field described by the Rabi frequency Ω_L, and we first study the case where this coupling field is kept constant. In order to avoid resonant coupling to individual modes of Eq. (17), we assume as well that the Ω_L field detuning from the single-atom resonance $|f\rangle - |e^{+1}\rangle$ is larger than the Rabi frequency Ω_L; see Sec. IV for further discussion.

We first consider a sample of $3 \times 3 \times 8$ atoms arranged in a lattice along the x, y, and z directions, respectively, with the lattice period $d \geqslant \lambda_0/2$. This case would correspond to trapping alkali atoms on the ω_0 transition in a red-detuned lattice.

The calculated emission of a single photon from this atomic sample is presented in Fig. 3. Figure 3(a) shows the intensity of the field, integrated over directions, at different distances from the atomic sample, i.e., $I = \sum_\epsilon \int d\Omega r^2 I_\epsilon(\vec{r},t)$. The field propagates at the speed of light, and this snapshot of the intensity distribution with distance reflects how the state $|f\rangle$ population has gradually decayed via the optically excited states since the coupling field was switched on. The most prominent feature is the overall exponentially decaying shape, but Fig. 3(a) also shows residual oscillation behavior. This modulation comes from off-resonant Rabi oscillations between states $|f_j\rangle$ and $|e_j^{+1}\rangle$. Figures 3(b) and 3(c) show the spatial intensity distribution $I_{\Omega,\epsilon} = r^2 I_\epsilon(\vec{r},t)$, indicated by different colors, for the same parameters as in Fig. 3(a). Figure 3(b) shows the intensity distribution for the polarization of the emitted light, which is expected to be dominant for the level scheme by the dipole selection rule. We observe that most of the light is emitted in a narrow forward peak. Figure 3(c) shows that in the backward direction, a small component (note the different color scale) is emitted with the opposite polarization, again in agreement with the atomic dipole selection rule. To quantify the angular distribution of the emitted light, Figs. 3(d) and 3(e) show polar plots of the intensity of the left-handed and right-handed light components at the distance $R = 199c/\Gamma$.

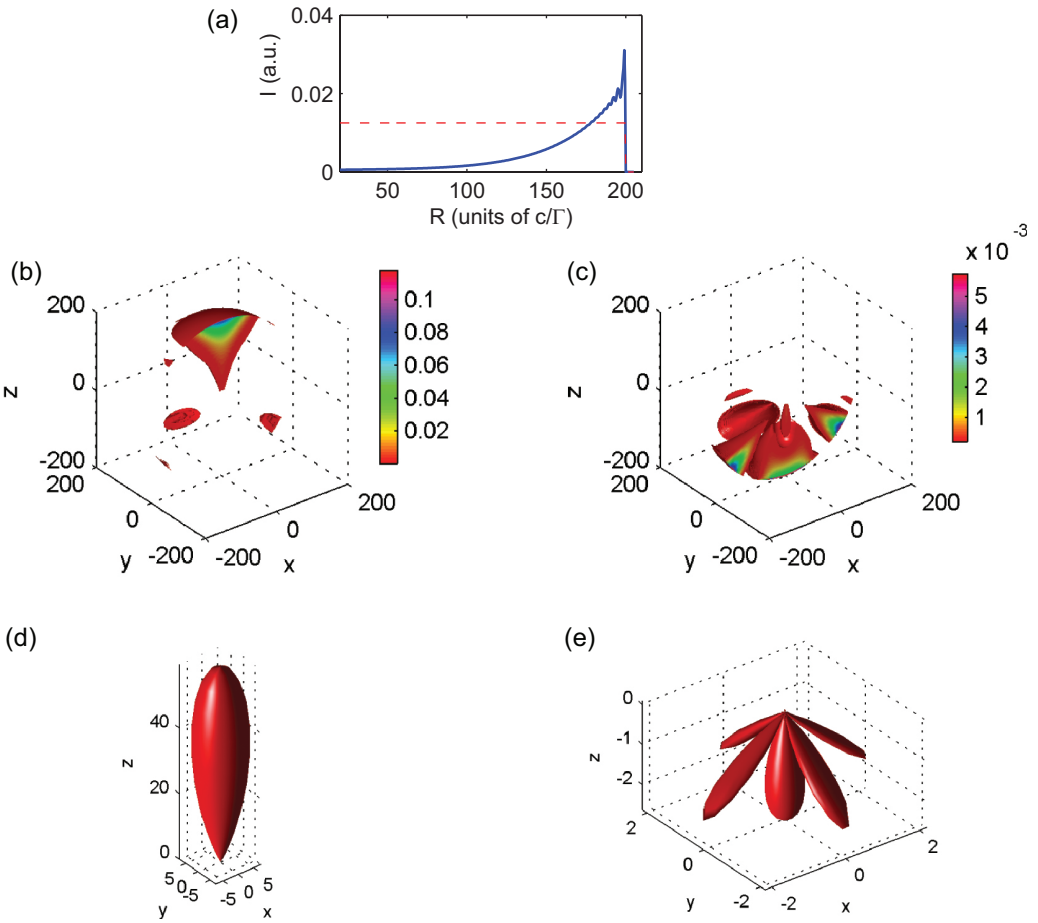

FIG. 3. (Color online) Emission of a single photon from a small atomic sample of $3 \times 3 \times 8$ atoms arranged in a lattice with the spacing $d = 0.60\lambda_0$. (a) Integrated intensity $I = \sum_\epsilon \int d\Omega r^2 I_\epsilon(\vec{r},t)$ as a function of the distance from the atomic sample (solid line) and the out-coupling pulse shape (dotted line). (b) Spatial distribution of intensity of left-handed polarized light $I_{\Omega,l} = r^2 I_l(\vec{r},t)$ for a given time $t = 200\lambda_0/c$. The spatial coordinates are given in units of c/Γ. (c) Same as (b), but for the opposite handedness of the light (right handed). The intensity scale is given in the same arbitrary units in (b) and (c). (d) Polar plot of the angular intensity distributions of light at $R = 199c/\Gamma$ corresponding to (b) at the moment of the maximum intensity. More than 95% of the intensity is emitted in the positive z direction within a cone with a half opening angle $\Delta\theta = 0.33$ rad. (e) The corresponding intensity distribution for the right-handed polarization. The same intensity units are applied for the two polarizations in (d) and (e) (note the values differ by an order of magnitude). The parameters used for this simulation are $\Omega_L = 2\Gamma$, and the single-atom detuning of the Ω_L field is 10Γ.

The directionality of the emitted light as a function of the lattice spacing was analytically studied by Porras and Cirac [42] for the case of two-level atoms. In this model the radiative pattern can be factorized into two parts: (1) collective scalar field radiative effects and (2) a dipole radiative pattern of individual atoms. Our calculations indicate that reabsorption effects and the inclusion of multiple excited states become important for the case of strongly coupled atoms with atomic spacings $d \approx 0.25\lambda_0$ and for the case of frustrated emission even with large atomic spacings (see Appendix B). In these cases atomic reabsorption of photons with a resulting redistribution of angular momentum does not justify a simple factorization in terms of a collective scalar and the dipole emission pattern.

Our calculations also show that for the case of forward emission for atoms with larger separations, the role of levels $|e_j^0\rangle$ and $|e_j^{-1}\rangle$ in the photon reabsorption effects is negligible. The directionality of emission in this case depends on the lattice spacing and can be understood as the interference of Bragg scattering contributions. For a critical spacing of $d = \lambda_0/2$ or an integer multiple of $\lambda_0/2$, the photon is mainly emitted in the forward and backward directions with equal probability; see Figs. 4(a) and 4(e). With an increased value of d this symmetry is broken, and the forward emission peak becomes dominant; see Figs. 4(b)–4(d) and 4(f). Due to the diffraction-like effects the directionality of the emitted light improves with the increase of the array size. Figures 4(c), 4(g), and 4(h) show the angular distribution of emitted light for lattices with the same spacing, but with an increasing number of atoms. This analysis confirms the observations made in Ref. [42].

In this section we have studied the collective emission of single photons, and we have analyzed the details of their directional distribution and their associated polarization properties. We have identified regimes where the full Zeeman manifold of the atomic excited state is important for photon

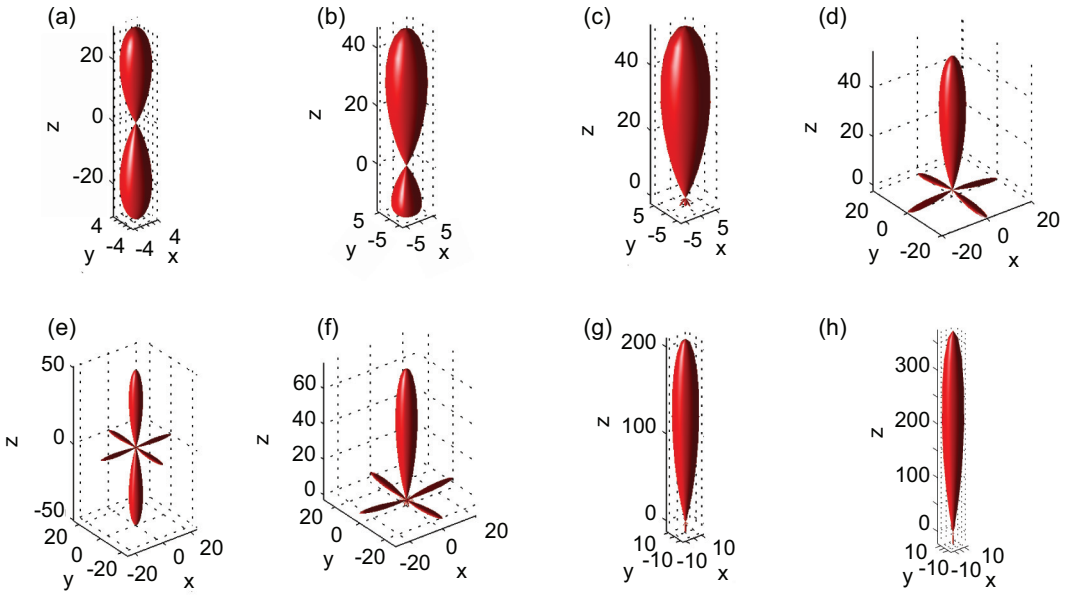

FIG. 4. (Color online) Polar plot of emitted light for a lattice of $3 \times 3 \times 8$ atoms for the cases (a) $d = 0.50\lambda_0$ ($\Delta\theta = 0.38$ rad), (b) $d = 0.53\lambda_0$ ($\Delta\theta = 0.36$ rad), (c) $d = 0.60\lambda_0$ ($\Delta\theta = 0.33$ rad), (d) $d = 0.90\lambda_0$ ($\Delta\theta = 0.22$ rad), (e) $d = 1.00\lambda_0$ ($\Delta\theta = 0.20$ rad), and (f) $d = 1.10\lambda_0$ ($\Delta\theta = 0.18$ rad). The total angular distribution for lattices (g) $6 \times 6 \times 8$ ($\Delta\theta = 0.21$ rad) and (h) $8 \times 8 \times 8$ ($\Delta\theta = 0.18$ rad) with $d = 0.60\lambda_0$. The coupling laser parameters are the same as in Fig. 3.

reabsorption effects and regimes where it can be neglected. In the next section we turn to the temporal shape of the emitted light pulses and to the experimental means to control the light mode of the emitted photon.

IV. TEMPORAL PHOTON MODES

The angular emission patterns shown in the previous section were all calculated assuming a constant intensity of the laser which drives the $f \leftrightarrow e$ transition. This leads to a highly asymmetric temporal profile of the emitted light, shown in Fig. 3(a). By controlling the temporal profile of the coupling $\Omega_L(t)$ one can control the temporal shape of the emitted light, and this can be used to transfer the atomic excitation from state $|f\rangle$ to, e.g., a temporary symmetric emitted photon wave packet. Such a wave packet can be reabsorbed in a second atomic ensemble if one employs the time-reversed control field. Therefore we may imagine a collection of atomic ensembles as quantum repeater stations, where photon pulses are absorbed and reemitted, possibly after suitable entanglement distillation and state purification [2,12].

To design appropriate out-coupling laser fields, we start with a system prepared in states $|f_j\rangle$ described by Eq. (20) with a vanishing coupling Ω_L. By gradually increasing the coupling strength we transfer the population to states $|e_j^{+1}\rangle$, which decay to the ground state by the emission of light. The intensity of the emitted light is given by the population of excited state $|e_j^{+1}\rangle$, and our goal is thus to control this population.

Due to the complexity of the nonorthogonal eigenmodes of the coupling Hamiltonian, we follow the approach in Sec. III and focus here on the conceptually easiest strategy, which is an *adiabatic* out-coupling. By introducing a detuning $\delta = \omega_{fe} - \omega_L$ and $\beta_l^{\nu} = \tilde{\beta}_l^{\nu} e^{-i\delta t}$ we can rewrite Eqs. (9) and (10):

$$\dot{a}_l = \frac{\Omega_L}{2i}\tilde{\beta}_l^{+1}, \tag{21}$$

$$\dot{\tilde{\beta}}_l^{+1} = \frac{\Omega_L}{2i}a_l + i\left(\delta + \Delta_{\mathrm{Lamb}}\right)\tilde{\beta}_l^{+1} - \frac{\Gamma}{2}\tilde{\beta}_l^{+1} - \frac{\Gamma}{2}\sum_{j=1,j\neq l}^{N}\left(\hat{d}_{+1,g}^{l}\cdot\overleftrightarrow{F}_{l,j}\cdot\hat{d}_{g,+1}^{j}\right)\tilde{\beta}_j^{+1}. \tag{22}$$

Since state $|f_j\rangle$ is coupled by a strong field Ω_L to $|e_j^{+1}\rangle$, whereas substates $|e_j^{-1}\rangle$ and $|e_j^{0}\rangle$ are only coupled by virtual photon processes to state $|e_j^{+1}\rangle$, we have neglected the populations of the $|e_j^{-1}\rangle$ and $|e_j^{0}\rangle$ substates. This approximation is justified for directed forward emission, as we have discussed in the previous section. Assuming further that the detuning δ is much larger than the Rabi frequency Ω_L, the single-atom decay rate Γ, and the Lamb shifts, we adiabatically eliminate state $\tilde{\beta}_l^{+1}$:

$$\tilde{\beta}_l^{+1} = \left(\frac{\Omega_L}{2\delta} - i\frac{\Gamma}{2\delta}\frac{\Omega_L}{2\delta}\right)a_l - i\frac{\Gamma}{2\delta}\sum_{j=1,j\neq l}^{N}\left(\hat{d}_{+1,g}^{l}\cdot\overleftrightarrow{F}_{l,j}\cdot\hat{d}_{g,+1}^{j}\right)\tilde{\beta}_j^{+1}. \tag{23}$$

We can see directly that the leading term of $\tilde{\beta}_l^{+1}$ is of the order $O(\frac{\Omega_L}{\delta})$ since a_l is of the order of 1. Therefore the population of state $|e_l^{+1}\rangle$ is always much smaller than unity and quickly decays to the ground state. Hence the intensity of the emitted light is approximately given by the population of state $|e_l^{+1}\rangle$. Substituting Eq. (23) into Eq. (21) and neglecting terms of

order higher than $O(\frac{\Gamma^3}{\delta^2})$, we arrive at a closed set of equations for the a coefficients:

$$\dot{a}_l = -i\,\Delta_{\text{light}} a_l - \frac{\Gamma'}{2} a_l - \frac{\Gamma'}{2} \sum_{j=1, j\neq l}^{N} (\hat{d}^l_{+1,g} \cdot \overleftrightarrow{F}_{l,j} \cdot \hat{d}^j_{g,+1}) a_j, \tag{24}$$

with the light shift $\Delta_{\text{light}} = \frac{\Omega_L^2}{4\delta}$ and the effective decay rate $\Gamma' = \Gamma \frac{\Omega_L^2}{4\delta^2}$ of the metastable state $|f_l\rangle$.

Similar to Eq. (22), the first line of this equation describes the dynamics of an isolated atom. The second line, which depends on the geometry, is the contribution from the interactions with all other atoms of the sample via virtual photon exchange processes. Since the collective contributions both in Eq. (22) and in Eq. (24) have the same form and the temporal evolution of the population $\tilde{\beta}_l^{+1}$ follows a_l as

$$\tilde{\beta}_l^{+1} = \frac{\Omega_L}{2\delta} a_l, \tag{25}$$

up to order $O(\frac{\Omega_L}{\delta})$, we conclude that the spatiotemporal mode function occupied by the emitted photon has the same structure, up to a radial scaling factor, as in the case studied in Sec. III.

In order to tailor the temporal dynamics of the emitted light, we now allow temporal modulation of the control field $\Omega_L(t) = \Omega_{L0} f(t)$, with $0 \leqslant f(t) \leqslant 1$, for all times. With this notation Eq. (24) becomes

$$\frac{1}{f(t)^2}\frac{da_l(t)}{dt} = -i\frac{\Omega_{L0}^2}{4\delta} a_l(t) - \frac{\Gamma}{2}\frac{\Omega_{L0}^2}{4\delta^2} a_l(t) - \frac{\Gamma}{2}\frac{\Omega_{L0}^2}{4\delta^2} \sum_{j=1, j\neq l}^{N} (\hat{d}^l_{+1,g} \cdot \overleftrightarrow{F}_{l,j} \cdot \hat{d}^j_{g,+1}) a_j(t). \tag{26}$$

In contrast to the resonant out-coupling case described by Vasilev *et al.* [50], in our adiabatic out-coupling case there is no general analytic solution of this equation. Nevertheless, we can find a connection between the solution $a_l^0(t)$ of Eq. (26) with a constant Ω_L, i.e., $f = 1$, and the solution $a_l(t)$ for an arbitrary $f(t)$. Defining

$$\tau(t) = \int_0^t f(t')^2 dt', \tag{27}$$

we observe that

$$b_l(\tau(t)) = a_l(t) \tag{28}$$

obeys the equation

$$\frac{db_l(\tau)}{d\tau} = -i\frac{\Omega_{L0}^2}{4\delta} b_l(\tau) - \frac{\Gamma}{2}\frac{\Omega_{L0}^2}{4\delta^2} b_l(\tau) - \frac{\Gamma}{2}\frac{\Omega_{L0}^2}{4\delta^2} \sum_{j=1, j\neq l}^{N} (\hat{d}^l_{+1,g} \cdot \overleftrightarrow{F}_{l,j} \cdot \hat{d}^j_{g,+1}) b_j(\tau). \tag{29}$$

Since this equation is identical to Eq. (26) for constant f, we directly obtain its formal solution $b_l(\tau) = a_l^0(\tau)$, and hence, the general solution to Eq. (26) reads

$$a_l(t) = a_l^0(\tau(t)). \tag{30}$$

That means the time evolution of $a_l(t)$ can be advanced or retarded with respect to $a_l^0(t)$ by choosing the appropriate function $f(t)$ in Eq. (27).

To calculate the temporal pulse shape $f(t)$ leading to any desired output intensity $I(t)$, we observe that the number of photons emitted under constant amplitude driving is related to the population in the initial atomic state,

$$n^0(t) \equiv \int_0^t dt' I^0(t') = 1 - \sum_{l=1}^{N} |a_l^0(t)|^2, \tag{31}$$

while the corresponding number of photons in the desired field is

$$n(t) \equiv \int_0^t dt' I(t') = 1 - \sum_{l=1}^{N} |a_l(t)|^2. \tag{32}$$

Equation (30) implies the equation for $\tau(t)$:

$$n(t) = n^0(\tau(t)). \tag{33}$$

Figure 5(a) shows the emitted intensities (thick dashed blue curve) obtained with a constant out-coupling amplitude

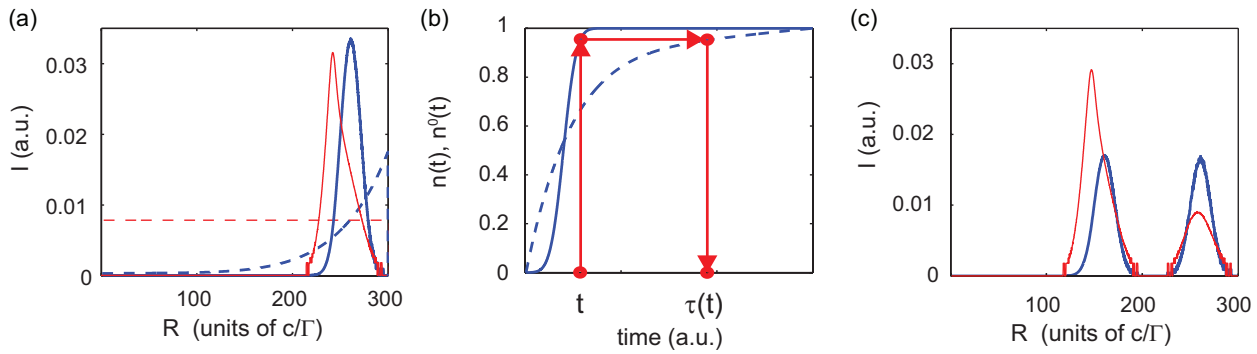

FIG. 5. (Color online) Temporal shaping of the photon emission from an atomic array of $3 \times 3 \times 8$ atoms with $d = 0.60\lambda_0$. (a) Output intensity (thick blue dashed line) using a constant pulse (thin red dashed line) with $\Omega_{L0} = 10.5\Gamma$ and $\delta = 120\Gamma$. With a specially designed out-coupling pulse with peak Rabi frequency $\Omega_{L0} = 42.0\Gamma$ and the temporal shape $f(t)$ (thin red solid line), we obtain a Gaussian temporal shape at $R = 260c/\Gamma$ of the emitted light intensity (thick blue solid line). (b) Integrated intensities $n^0(t)$ (dashed line) and $n(t)$ (thick solid curve) and a graphical solution (red arrows) of the equation $n(t) = n^0(\tau(t))$. (c) Out-coupling of a double-peaked pulse (thick blue line) using $\Omega_{L0} = 38.85\Gamma$ and $f(t)$ (thin red line).

(thin dashed red curve) and a Gaussian pulse with $1/e$ width $15\Gamma^{-1}$ at $R = 260c/\Gamma$ (thick solid blue curve) obtained with the calculated amplitude $f(t)$ (thin solid red curve), respectively. The corresponding integrated intensities are shown in Fig. 5(b), which also illustrates the numerical procedure to solve (33) and establish the correspondence between the values $\tau(t)$ and t, as indicated by the red arrows. By numerically differentiating the function $\tau(t)$ and using Eq. (27) we directly obtain the temporal profile of the out-coupling pulse $f(t)$ leading to the desired $I(t)$. This function is shown as a thin solid red curve in Fig. 5(a); the spikes are due to precision errors in the calculation of the derivative of $\tau(t)$. We insert this out-coupling pulse into our simulation of the *full coupled equations*, and we calculate the resulting emitted intensity which is, indeed, the result, presented as the thick solid blue line in Fig. 5(a). To demonstrate our ability to couple out arbitrary pulse shapes, we aim in Fig. 5(c) at a double-peaked pulse with equal heights at $R = 160c/\Gamma$ and $R = 260c/\Gamma$. The corresponding profile of $f(t)$ is shown as a thin red line in Fig. 5(c), and again, the thick solid blue curve shows the outcome of the simulation of the full set of coupled atomic equations.

We presented here a recipe for photon shaping starting from a constant amplitude control pulse. Using this as a reference, it is possible to relate the outcome of different control pulses by a suitable parametrization of the time argument and to use the above method with experimentally measured intensities. While we assumed a varying amplitude but a constant phase of the control field $\Omega_L(t)$ to produce more complicated single-photon wave packets, it may be worthwhile to study also complex-valued $f(t)$.

V. CONCLUSION

We studied correlated spontaneous emission from small arrays of atoms. Our atomic model is the simplest generalization of a two-level atom, which allows us to fully account for polarization effects. Numerically solving the equations of motion, we demonstrated the possibility of deterministically generating single photons with a well-defined spatial emission profile, which can be controlled by the geometry of the array. Moreover, we established a method to shape the temporal dependence of the photon wave packets at will. In particular, the method allows us to prepare time-symmetric wave packets, which may be sent from one atomic ensemble and absorbed by another with manageable time-reversed control fields on the two ensembles, thus considerably simplifying the experimental procedures needed for application in quantum communication networks.

The results of this work pave the way towards an experimental realization of quantum repeaters based on cold neutral atoms. Each node may be a sample of cold alkali, alkaline-earth, or rare-earth atoms arranged in a three-dimensional array. Such arrays, e.g., with rubidium, strontium, or ytterbium atoms, can now be routinely created using standing waves of counterpropagating laser beams. The typical spacings in these arrays range from half the optical wavelength and upwards for red-detuned traps, and they readily satisfy the requirements for directional emission even for small atomic samples. At the same time in such samples the maximum distance between any two atoms may be kept smaller than the Rydberg blockade radius, allowing us to initialize the system with exactly one excitation. The buffer $|f\rangle$ state might directly be the Rydberg state, which has a lifetime three orders of magnitude longer than the $|e^{+1}\rangle$ state, or it may be one of the states of the ground-state manifold [42].

Finally, we also studied the atomic emission dynamics in the case where the emission is frustrated, i.e., when the phase-matching condition favors emission in directions forbidden by the dipole emission pattern and in the case of denser systems with $d < \lambda/2$. In both cases the Zeeman sublevels of the excited state contribute to the subradiant modes. The experimental realization of conditions to observe these effects will require arrays of alkaline-earth or rare-earth atoms in blue- or red-detuned optical lattices.

ACKNOWLEDGMENTS

We acknowledge financial support from the EU Integrated Project AQUTE and from the project MALICIA under FET-Open Grant No. 265522.

APPENDIX A

We derive the explicit dependence of $I_\epsilon(\vec{r},t)$ on the atomic part β of the wave function. We rewrite first Eq. (18) as [49]

$$I_\epsilon = \langle\psi|E_\epsilon^{(-)}|g\rangle|0\rangle\langle 0|\langle g|E_\epsilon^{(+)}|\psi\rangle. \tag{A1}$$

The photon "wave function" is

$$\begin{aligned}|\Psi_\epsilon\rangle &= \langle 0|\langle g|\langle 0|E_\epsilon^{(+)}(\vec{r})\,|\psi(t)\rangle \\ &= i\sum_{\vec{k}}\sum_{\lambda}\varepsilon_k(\vec{\epsilon}\cdot\vec{\epsilon}_{\vec{k},\lambda})e_{\vec{k},\lambda}e^{i(\vec{k}\cdot\vec{r}-\omega_k t)},\end{aligned} \tag{A2}$$

with $e_{\vec{k},\lambda}$ from Eq. (8).

As the second step, we simplify this expression. The summation over polarizations is performed using a recipe from the Appendix of Smith *et al.* [51]:

$$\begin{aligned}|\Psi_\epsilon\rangle = i\sum_{\vec{k}}\sum_{j=1}^{N}\sum_{\nu=-1}^{1}&\left[\vec{\epsilon}\cdot(\overleftrightarrow{I}-\hat{k}\hat{k})\cdot\hat{d}_{g\nu}^{j}\right] \\ &\times\varepsilon_k g_k e^{i(\vec{k}\cdot\vec{R}_j-\omega_k t)}\int_0^t d\tau\beta_j^\nu(\tau)e^{-i(\omega_0-\omega_k)\tau},\end{aligned} \tag{A3}$$

with $\vec{R}_j = \vec{r} - \vec{r}_j$. After replacing the summation over the wave vectors $\sum_{\vec{k}}$ by an integral $\frac{V}{(2\pi c)^3}\int_0^\infty d\omega_k\omega_k^2\int d\Omega(k)$, we get

$$\begin{aligned}|\Psi_\epsilon\rangle = i\sum_{j=1}^{N}\sum_{\nu=-1}^{1}&\frac{V}{(2\pi c)^3}\int_0^\infty d\omega_k\omega_k^2\varepsilon_k g_k e^{-i\omega_k t} \\ &\times\int_0^t d\tau\beta_j^\nu(\tau)e^{-i(\omega_0-\omega_k)\tau} \\ &\times\int d\Omega(k)\left[\vec{\epsilon}\cdot(\overleftrightarrow{I}-\hat{k}\hat{k})\cdot\hat{d}_{j\nu}^{j}\right]e^{i\vec{k}\cdot\vec{R}_j}.\end{aligned} \tag{A4}$$

The angular integration can already be performed at this step [51], resulting in

$$|\Psi_\epsilon\rangle = i\sum_{j=1}^{N}\sum_{\nu=-1}^{1}\frac{V}{(2\pi c)^3}\int_0^\infty d\omega_k\omega_k^2\varepsilon_k g_k e^{-i\omega_k t} \times\int_0^t d\tau\beta_j^\nu(\tau)e^{-i(\omega_0-\omega_k)\tau}4\pi\left[\vec{\epsilon}\cdot\overleftrightarrow{\zeta}(kR_j)\cdot\hat{d}_{j\nu}^{j}\right], \tag{A5}$$

with $\overleftrightarrow{\zeta}(kR) = (\overleftrightarrow{I} - \hat{R}\hat{R})\frac{\sin(kR)}{kR} + O(\frac{1}{(kR)^2})$ [51]. Therefore the photon intensity up to the order of $O((kR)^{-2})$, with $r \gg r_j$, is

$$|\Psi_\epsilon\rangle = \sum_{j=1}^{N}\sum_{\nu=-1}^{1}B_{\hat{r},j}^{\nu}\frac{1}{R_j}\int_0^t d\tau\beta_j^\nu(\tau)e^{-ick_0\tau} \times\int_0^\infty dk k^2[e^{ikR_j+ick(\tau-t)} - e^{-ikR_j+ick(\tau-t)}], \tag{A6}$$

where we have introduced $B_{\hat{r},j}^{\nu} = \frac{1}{4\pi\varepsilon_0}\frac{c}{2\pi}d_{eg}[\vec{\epsilon}\cdot(\overleftrightarrow{I} - \hat{R}_j\hat{R}_j)\cdot\hat{d}_{g\nu}^{j}]$. Since during the emission the value of k is peaked around the atomic resonance k_0 where the last time integral is relevant, we can replace k^2 with k_0^2 and extend the lower integral limit to $-\infty$ [49], i.e., the Weisskopf-Wigner approximation. Using the definition of the δ function $\delta(t) = \frac{1}{2\pi}\int_{-\infty}^{\infty}dke^{ikt}$, Eq. (A6) becomes

$$|\Psi_\epsilon\rangle = \sum_{j=1}^{N}\sum_{\nu=-1}^{1}B_{\hat{r},j}^{\nu}\frac{2\pi}{c}\frac{k_0^2}{R_j} \times\left[\int_0^t d\tau\beta_j^\nu(\tau)e^{-ick_0\tau}\delta\left(t-\frac{R_j}{c}-\tau\right) - \int_0^t d\tau\beta_j^\nu(\tau)e^{-ick_0\tau}\delta\left(t+\frac{R_j}{c}-\tau\right)\right]. \tag{A7}$$

Since the last integral with the δ function is always zero, we arrive at

$$|\Psi_\epsilon\rangle = \sum_{j=1}^{N}\sum_{\nu=-1}^{1}\frac{d_{eg}k_0^2}{4\pi\varepsilon_0 R_j}\beta_j^\nu\left(t-\frac{R_j}{c}\right)e^{-ick_0\left(t-\frac{R_j}{c}\right)} \times\left[\vec{\epsilon}\cdot(\overleftrightarrow{I} - \hat{R}_j\hat{R}_j)\cdot\hat{d}_{g\nu}^{j}\right]. \tag{A8}$$

Finally, we arrive at the desired explicit dependence of the photon intensity on the atomic part β:

$$I_\epsilon(\vec{r},t) = \langle\Psi_\epsilon|\Psi_\epsilon\rangle = \frac{d_{eg}^2k_0^4}{(4\pi\varepsilon_0 r)^2}\sum_{j,j'=1}^{N}\sum_{\nu,\sigma=-1}^{1}\beta_j^\nu\left(t-\frac{r}{c}\right)\left[\beta_{j'}^\sigma\left(t-\frac{r}{c}\right)\right]^* \times e^{ik_0[\hat{r}\cdot(\vec{r}_j-\vec{r}_{j'})]}\left[\vec{\epsilon}\cdot(\overleftrightarrow{I} - \hat{R}_j\hat{R}_j)\cdot\hat{d}_{g\nu}^{j}\right] \times\left[\vec{\epsilon}\cdot(\overleftrightarrow{I} - \hat{R}_{j'}\hat{R}_{j'})\cdot\hat{d}_{\sigma g}^{j'}\right], \tag{A9}$$

where we have used $R_j \approx r$ for β and in the denominator but kept the significant term $R_j = r - (\hat{r}\cdot\vec{r}_j)$ in the exponents.

This equation allows a very transparent physical interpretation for the case of many noninteracting atoms. We suppose states $|f_j\rangle$ are fully mapped onto the corresponding $|e_j^{+1}\rangle$, i.e., $a_j = 0$ in Eq. (7). Therefore the atomic evolution is described by

$$\beta_j^{+1}(t) = \frac{1}{\sqrt{N}}e^{-i\vec{k}_{em}\cdot\vec{r}_j}e^{-\frac{\Gamma}{2}t}, \quad \beta_j^0(t) = 0, \tag{A10}$$

and

$$\beta_j^{-1}(t) = 0,$$

which is the solution of Eq. (10) for $k_0R_{l,j} \gg 1$, i.e., vanishing coupling $\overleftrightarrow{F}_{l,j}$. The wave vector $\vec{k}_{em}$ is defined in Fig. 1. The

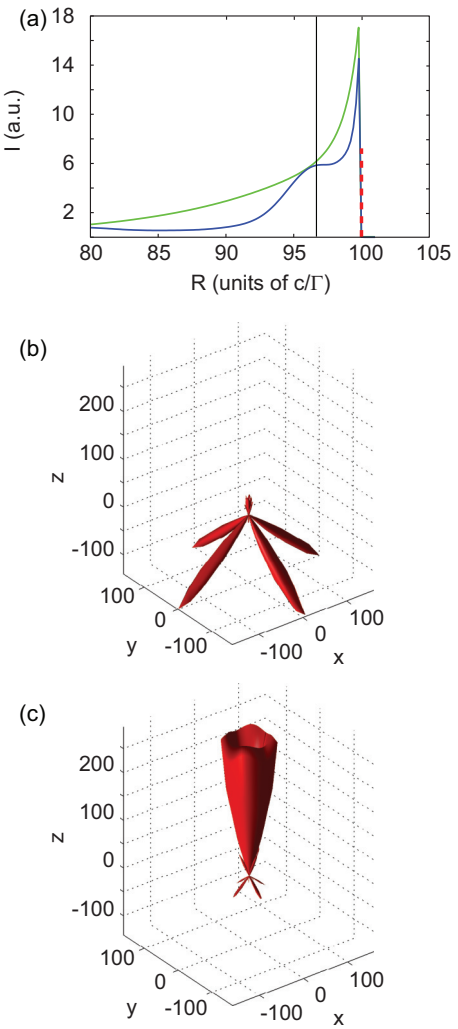

FIG. 6. (Color online) Frustrated emission from a sample of $6 \times 6 \times 12$ atoms with the lattice spacing $d = 0.60\lambda_0$. (a) A snapshot of the angularly integrated intensity of the emitted light after excitation with a short pulse (red dashed line) with the same parameters as in Fig. 2. The case where all $|e^{-1}\rangle$, $|e^0\rangle$, and $|e^{+1}\rangle$ levels are included is shown with the blue (dark gray) curve, and the case restricted to a single excited state $|e^0\rangle$ is shown with the green (light gray) curve. Angular distribution at $R = 96.6c/\Gamma$ (b) for the case of the full manifold of the excited state and (c) for the case restricted to $|e^0\rangle$.

corresponding emitted intensity is then

$$I_\epsilon(\vec{r},t) = \frac{d_{eg}^2 k_0^4}{(4\pi\varepsilon_0 r)^2 N} e^{-\Gamma(t-\frac{r}{c})} \sum_{j=1}^{N} C_{j,j}^{\epsilon} + \frac{d_{eg}^2 k_0^4}{(4\pi\varepsilon_0 r)^2 N} \times e^{-\Gamma(t-\frac{r}{c})} \sum_{j=1}^{N}\sum_{j'=1}^{N} (1-\delta_{j,j'}) C_{j,j'}^{\epsilon} e^{i(k_0\hat{r}-\vec{k}_{em})\cdot(\vec{r}_j-\vec{r}_{j'})}, \tag{A11}$$

with

$$C_{j,j'}^{\epsilon} = \left[\vec{\epsilon}\cdot(\overleftrightarrow{I} - \hat{R}_j\hat{R}_j)\cdot\hat{d}_{g,+1}^{j}\right]\left[\vec{\epsilon}\cdot(\overleftrightarrow{I} - \hat{R}_{j'}\hat{R}_{j'})\cdot\hat{d}_{+1,g}^{j'}\right]. \tag{A12}$$

Equation (A12) can be further simplified using $\hat{R}_j\hat{R}_j = \hat{r}\hat{r}[1+O(\frac{r_j}{r})]$ and assuming that all dipoles are polarized in the same direction, i.e., $\hat{d}_{g,+1}^{j} = \hat{d}_{g,+1}$. In this case the function $C_{j,j}^{\epsilon}$ has an interpretation as the angular dependence of the dipole emission pattern for a given helicity ϵ expressed in a tensor form. In particular, if we introduce a spherical coordinate system along the $\hat{d}_{g,0}$ direction and sum over all polarizations, we arrive at the well-known dipole pattern angular dependence $\frac{1}{2}(1+\cos^2\theta)$ for a dipole emitting on the $|e^{+1}\rangle \to |g\rangle$ transition.

Correspondingly, in the direction $\hat{r} = \frac{\vec{k}_{em}}{k_0}$ we have

$$I_\epsilon(\vec{r},t) \approx N^2 \times \frac{d_{eg}^2 k_0^4}{N(4\pi\varepsilon_0 r)^2} e^{-\Gamma(t-\frac{r}{c})} C_{j,j}^{\epsilon}, \tag{A13}$$

while for all other directions $\hat{r} \neq \frac{\vec{k}_{em}}{k_0}$ the exponents in Eq. (A11) average out and give

$$I_\epsilon(\vec{r},t) \approx 1 \times \frac{d_{eg}^2 k_0^4}{N(4\pi\varepsilon_0 r)^2} e^{-\Gamma(t-\frac{r}{c})} C_{j,j}^{\epsilon}, \tag{A14}$$

i.e., $1/N^2$ reduced emission intensity. This is the well-known mechanism of *directed emission* from an atomic sample. Note as well that in this example, and in the more general case of spin-polarized two-level atoms, i.e., no coupling of $\nu = +1$ states to the other $\nu = 0,-1$ states, the single-atom dipole emission pattern factorizes out in the intensity formula (A9), as was pointed out by Porras and Cirac [42]. Nevertheless, this is not true in the general case considered here due to coupling of the $\nu = 0,-1$ levels to the level $\nu = +1$ via virtual photons [47].

APPENDIX B

We consider here the emission by an array of $6\times6\times12$ atoms with the spacing $d = 0.60\lambda_0$. The atoms are initially prepared in the timed Dicke superposition state of the $|f\rangle$ levels [Eq. (20)] as in all previous examples. This state favors emission in the z direction, but the storage level $|f\rangle$ is now coupled to the short-lived state $|e^0\rangle$. This state can directly decay to the ground state with the emission of a π-polarized photon, relative to the z axis; see Fig. 1. Since the angular emission pattern of this transition has zero intensity in the z direction, which is the preferred emission direction of this atomic sample, we obtain a conflict between the preferred and the allowed emissions. An example of the resulting frustrated emission is presented in Fig. 6. Here we plot a snapshot of the integrated intensity emitted by the atomic array out-coupled by a short pulse Ω_L (dashed red line) with the same parameters as in Fig. 2. The blue (dark gray) curve corresponds to the case with all $|e^{-1}\rangle$, $|e^0\rangle$, and $|e^{+1}\rangle$ levels included, whereas the green (light gray) curve corresponds to the manifold restricted to the $|e^0\rangle$ state. Figures 6(b) and 6(c) show the polar plots of the emitted radiation at $R = 96.6c/\Gamma$ for the two cases. The qualitatively different behavior in these two cases demonstrates the importance of the inclusion of the full manifold of the states. This difference stems from the reabsorption of virtual photons with different polarizations.

[1] S. Olmschenk, D. Hayes, D. N. Matsukevich, P. Maunz, D. L. Moehring, and C. Monroe, Int. J. Quantum Inf. **8**, 337 (2010).

[2] L.-M. Duan, M. D. Lukin, J. I. Cirac, and P. Zoller, Nature (London) **414**, 413 (2001).

[3] L. Hau, S. Harris, Z. Dutton, and C. Behroozi, Nature (London) **397**, 594 (1999).

[4] A. Kuzmich, K. Mølmer, and E. S. Polzik, Phys. Rev. Lett. **79**, 4782 (1997).

[5] K. Hammerer, A. S. Sørensen, and E. Polzik, Rev. Mod. Phys. **82**, 1041 (2010).

[6] U. Schnorrberger, J. D. Thompson, S. Trotzky, R. Pugatch, N. Davidson, S. Kuhr, and I. Bloch, Phys. Rev. Lett. **103**, 033003 (2009).

[7] A. T. Black, J. K. Thompson, and V. Vuletic, Phys. Rev. Lett. **95**, 133601 (2005).

[8] Y. O. Dudin and A. Kuzmich, Science **336**, 887 (2012).

[9] M. Bonarota, J.-L. Le Gouët, and T. Chaneliere, New J. Phys. **13**, 013013 (2011).

[10] I. Usmani, M. Afzelius, H. de Riedmatten, and N. Gisin, Nat. Commun. **1**, 12 (2010).

[11] M. Afzelius, I. Usmani, A. Amari, B. Lauritzen, A. Walther, C. Simon, N. Sangouard, J. Minar, H. de Riedmatten, N. Gisin, and S. Kroll, Phys. Rev. Lett. **104**, 040503 (2010).

[12] N. Gisin and R. Thew, Nat. Photonics **1**, 165 (2007).

[13] K. C. Lee, M. R. Sprague, B. J. Sussman, J. Nunn, N. K. Langford, X.-M. Jin, T. Champion, P. Michelberger, K. F. Reim, D. England, D. Jaksch, and I. A. Walmsley, Science **334**, 1253 (2011).

[14] M. Keller, B. Lange, K. Hayasaka, W. Lange, and H. Walther, New J. Phys. **6**, 95 (2004).

[15] A. Kuhn and D. Ljunggren, Contemp. Phys. **51**, 289 (2010).

[16] A. D. Boozer, A. Boca, R. Miller, T. E. Northup, and H. J. Kimble, Phys. Rev. Lett. **98**, 193601 (2007).

[17] M. Albert, A. Dantan, and M. Drewsen, Nat. Photonics **5**, 633 (2011).

[18] K. Hennessy, A. Badolato, M. Winger, D. Gerace, M. Atatüre, S. Gulde, S. Fält, E. Hu, and A. Imamoglu, Nature (London) **445**, 896 (2007).

[19] J. S. Neergaard-Nielsen, B. M. Nielsen, C. Hettich, K. Mølmer, and E. S. Polzik, Phys. Rev. Lett. **97**, 083604 (2006).

[20] K. S. Choi, A. Goban, S. B. Papp, S. J. van Enk, and H. J. Kimble, Nature (London) **468**, 412 (2010).
[21] W. Jiang, Ch. Han, P. Xue, L.-M. Duan, and G.-C. Guo, Phys. Rev. A **69**, 043819 (2004).
[22] L. H. Pedersen and K. Mølmer, Phys. Rev. A **79**, 012320 (2009).
[23] M. Stobinska, G. Alber, and G. Leuchs, Europhys. Lett. **86**, 14007 (2009).
[24] M. D. Lukin, M. Fleischhauer, R. Cote, L. M. Duan, D. Jaksch, J. I. Cirac, and P. Zoller, Phys. Rev. Lett. **87**, 037901 (2001).
[25] M. Saffman, T. G. Walker, and K. Mølmer, Rev. Mod. Phys. **82**, 2313 (2010).
[26] M. Saffman and T. G. Walker, Phys. Rev. A **66**, 065403 (2002).
[27] A. Gaætan, Y. Miroshnychenko, T. Wilk, A. Chotia, M. Viteau, D. Comparat, P. Pillet, A. Browaeys, and P. Grangier, Nat. Phys. **5**, 115 (2009).
[28] E. Urban, T. A. Johnson, T. Henage, L. Isenhower, D. D. Yavuz, T. G. Walker, and M. Saffman, Nat. Phys. **5**, 110 (2009).
[29] Y. O. Dudin, L. Li, F. Bariani, and A. Kuzmich, Nat. Phys. **8**, 790 (2012).
[30] E. Brion, L. H. Pedersen, and K. Mølmer, J. Phys. B **40**, S159 (2007).
[31] E. Brion, L. H. Pedersen, M. Saffman, and K. Mølmer, Phys. Rev. Lett. **100**, 110506 (2008).
[32] R. Dicke, Phys. Rev. **93**, 99 (1953).
[33] R. Lehmberg, Phys. Rev. A **2**, 883 (1970).
[34] P. Milloni and P. Knight, Phys. Rev. A **10**, 1096 (1974).
[35] E. R. Buley and F. W. Cummings, Phys. Rev. **134**, A1454 (1964).
[36] N. Rehler and J. Eberly, Phys. Rev. A **3**, 1735 (1971).
[37] J. Manassah, Phys. Rep. **101**, 359 (1983).
[38] A. Svidzinsky and J. T. Chang, Phys. Rev. A **77**, 043833 (2008).
[39] A. A. Svidzinsky, J. T. Chang, and M. O. Scully, Phys. Rev. A **81**, 053821 (2010).
[40] I. E. Mazets and G. Kurizki, J. Phys. B **40**, F105 (2007).
[41] M. O. Scully, E. S. Fry, C. H. R. Ooi, and K. Wodkiewicz, Phys. Rev. Lett. **96**, 010501 (2006).
[42] D. Porras and J. I. Cirac, Phys. Rev. A **78**, 053816 (2008).
[43] T. Bienaime, N. Piovella, and R. Kaiser, Phys. Rev. Lett. **108**, 123602 (2012).
[44] F. Bariani and T. A. B. Kennedy, Phys. Rev. A **85**, 033811 (2012).
[45] F. Bariani, Y. O. Dudin, T. A. B. Kennedy, and A. Kuzmich, Phys. Rev. Lett. **108**, 030501 (2012).
[46] Y. Li, J. Evers, H. Zheng, and S. Y. Zhu, Phys. Rev. A **85**, 053830 (2012).
[47] Y. Miroshnychenko and K. Mølmer (unpublished).
[48] M. Trippenbach, B. Gao, J. Cooper, and K. Burnett, Phys. Rev. A **45**, 6539 (1992).
[49] M. Scully and M. Zubary, *Quantum Optics* (Cambridge University Press, Cambridge, 1997).
[50] G. Vasilev, D. Ljunggren, and A. Kuhn, New J. Phys. **12**, 063024 (2010).
[51] M. Smith and K. Burnett, J. Opt. Soc. Am. B **8**, 1592 (1991).